We are IntechOpen, the world's leading publisher of Open Access books Built by scientists, for scientists

6,900
Open access books available

185,000
International authors and editors

200M
Downloads

Our authors are among the

154
Countries delivered to

TOP 1%
most cited scientists

12.2%
Contributors from top 500 universities



WEB OF SCIENCE™

Selection of our books indexed in the Book Citation Index in Web of Science™ Core Collection (BKCI)

Interested in publishing with us?
Contact book.department@intechopen.com

Numbers displayed above are based on latest data collected.
For more information visit www.intechopen.com



5

Crystallization in Microemulsions: A Generic Route to Thermodynamic Control and the Estimation of Critical Nucleus Size

Sharon Cooper, Oliver Cook and Natasha Loines
Durham University
UK

1. Introduction

Crystallization is ubiquitous. It is evident in natural processes such as biomineralization and gem formation, and is important in industrial processes both as a purification step and in the production of materials with specific properties, including drug polymorphs, cocrystals, mesocrystals, quasicrystals, quantum dots and other inorganic nanocrystals. Consequently it is essential to gain greater understanding of the process to be able to elicit more control over its outcome.

Crystallization occurs from melts that are supercooled, i.e. cooled below their equilibrium melting temperatures, T_{eq}. For crystallization from solution, the solutions must be supersaturated, i.e. have solute concentrations above their saturation values, c_{eq}, defined as the solute concentration in equilibrium with the macroscopic crystal. The supersaturation is the driving force for crystallization, being the difference in chemical potential, $\Delta\mu$, between the parent (melt or solution) and daughter (new crystal) phases. For crystallization from the melt, $\Delta\mu = \Delta_{fus}H\Delta T / T_{eq}$, where $\Delta_{fus}H$ is the enthalpy of fusion and ΔT = T_{eq} -T, is the supercooling with T denoting the temperature. Here it is assumed that $\Delta_{fus}H$ is invariant between T and T_{eq}. For an ideal solution, the supersaturation is $\Delta\mu = kT\ln\left(c / c_{eq}\right)$, where k is the Boltzmann constant, and c/c_{eq}, is the ratio of the solute concentration compared to its saturation value, which is known as the supersaturation ratio.

The formation of any new phase from a bulk parent phase requires the creation of an interface between the two phases, which requires work. Hence there exists an energy barrier to the formation of the new phase. The process of overcoming this energy barrier is known as nucleation. In crystallization, once nucleation has occurred, crystal growth onto the nuclei proceeds until the supersaturation is relieved. Owing to this nucleation stage, crystallization from the bulk melt or solution is typically under kinetic control, with metastable forms often crystallizing initially in accordance with Ostwald's rule of stages (Ostwald, 1897). In contrast, microemulsions have the unique ability to generically exert thermodynamic control over the crystallization process. This provides significant advantages; the size of the critical nucleus can be estimated with good accuracy under thermodynamic control conditions and importantly, the stable form of a material can be identified and readily

produced under ambient conditions. In this chapter we discuss the scientific rationale for this thermodynamic control and provide practical examples.

2. Theoretical considerations

2.1 Classical Nucleation Theory (CNT)

Nucleation can be modelled most simply using classical nucleation theory (CNT). Gibbs thermodynamic treatment of liquid nucleation from a vapour (Gibbs, 1876, 1878) shows that the free energy change, ΔF, involved in producing a spherical liquid nucleus from the vapour is given by:

$$\Delta F = -n\Delta\mu + \gamma A = -\frac{4\pi r^3 \Delta\mu}{3v_c} + 4\pi r^2 \gamma \tag{1}$$

where n is the number of molecules in the nucleus, $\Delta\mu$ denotes the chemical potential difference between the vapour and the liquid nucleus which defines the supersaturation, γ denotes the surface tension between the nucleus and the surrounding vapour, A denotes the surface area of the nucleus, r denotes its radius and v_c denotes the molecular volume of the new condensed phase, i.e. the liquid. This same thermodynamic treatment is often used for crystallization. For crystallization from bulk solutions at constant pressure, the relevant free energy to use is the Gibbs free energy. For crystallization from microemulsions, however, there is a very small Laplace pressure difference across the microemulsion droplet interface and so the Helmholtz free energy for constant volume systems is the appropriate free energy to employ.

Equation (1) clearly shows that the favourable formation of the bulk new phase in any supersaturated system, given by the first term $-n\Delta\mu$, is offset by the unfavourable surface free energy term, γA, that necessarily arises from creating the new interface. The surface free energy term dominates at smaller nucleus sizes and leads to the nucleation energy barrier (see Figure 1a). In particular, differentiating equation (1) with respect to r leads to a maximum at

$$r^* = 2\gamma v_c / \Delta\mu , \tag{2}$$

i.e. the well-known Gibbs-Thomson equation, with the nucleation barrier given by:

$$\Delta F^* = \frac{16}{3\Delta\mu^2}\pi\gamma^3 {v_c}^2 . \tag{3}$$

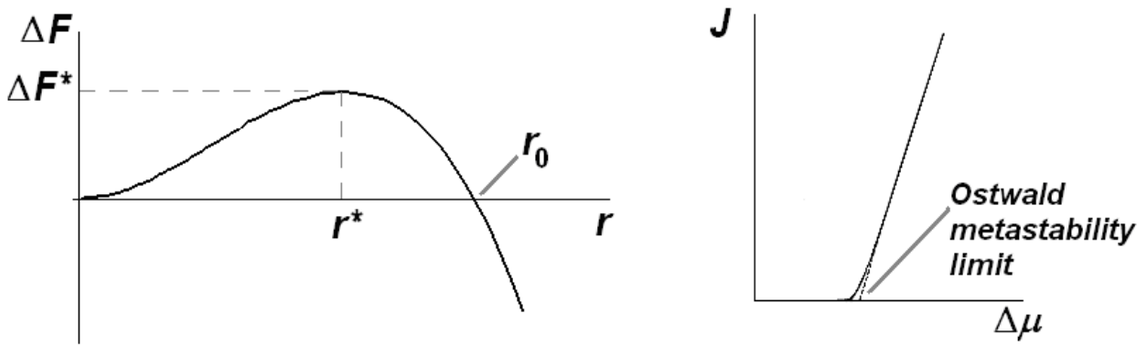
The r^* nucleus is termed the critical nucleus. It is of pivotal importance in CNT because it determines the size above which it is favourable for the new phase to grow. Nuclei smaller than r^* have a greater tendency to dissolve (or melt) than grow, whilst nuclei larger than r^* will tend to grow. The r^* nucleus has an equal probability of growing or dissolving (melting) and is in an unstable equilibrium with the surrounding solution (or melt). At larger r, a stable r_0 nucleus with $\Delta F = 0$ occurs (see Figure 1a).

Equation (3) gives the magnitude of the nucleation barrier when the new phase forms within the bulk parent phase, which is known as homogeneous nucleation. If the new phase

forms on a foreign surface, however, heterogeneous nucleation occurs. The corresponding heterogeneous nucleation barrier, ΔF_{het} that arises from forming a cap-shaped critical nucleus with a contact angle, θ, on the foreign surface is given by:

$$\Delta F^*_{het} = \frac{16\pi\gamma^3 {v_c}^2}{3\Delta\mu^2} f(\theta) = \Delta F^*_{hom} \frac{v^*_{het}}{v^*_{hom}} \tag{4}$$

where: ΔF^*_{hom} denotes the homogeneous nucleation barrier of the system given by equation (3), $f(\theta) = (2 - 3\cos\theta + \cos^3\theta)/4$ and v^*_{het} and v^*_{hom} denote the volumes of the heterogeneous and corresponding homogeneous critical nuclei, respectively. Note that equation (4) ignores the entropic free energy contribution arising from the number of surface sites upon which the nucleus may form, as this factor is incorporated in the pre-exponential factor, Ω, instead.



(a) (b)

Fig. 1. (a) Schematic graph of free energy change, ΔF vs. nucleus size, r, for a homogeneously nucleating crystal showing the critical nucleus, r^*, and stable nucleus, r_0, sizes. (b) Schematic graph of nucleation rate, J, vs. supersaturation, $\Delta\mu$, showing the Ostwald metastability limit which gives the onset crystallization temperature, T_c.

The kinetic theory of CNT (Volmer & Weber, 1926; Becker & Döring, 1935) used the nucleation barrier, ΔF^*, in an Arrhenius-type equation to derive the nucleation rate, J as:

$$J = \Omega \exp\left(-\Delta F^*/kT\right) \tag{5}$$

where Ω is the pre-exponential factor accounting for the rate at which the molecules impinge upon, and are incorporated into, the critical nuclei. The form of equation (5) is such that J remains negligibly small until the supersaturation reaches a critical value, the Ostwald metastability limit, at which point J suddenly and dramatically increases (see Figure 1b). Hence, an onset crystallization temperature, T_c, can be identified with this metastability limit, and the corresponding nucleation rate can be set, with little loss in accuracy, to a suitable detection limit for the technique monitoring the crystallization.

CNT is widely adopted because of its simplicity. However this simplicity limits its ability to model real systems. Two main assumptions are: firstly that it considers the nuclei to be spherical with uniform density and a structure equivalent to the bulk phase, and secondly

that the nuclei interfaces are infinitely sharp and have the same interfacial tensions as found at the corresponding planar interfaces. A recent review by Erdemir et al., 2009, details all the assumptions of CNT, and its applicability to different systems. Notably, given that CNT stems from the condensation of a liquid from its vapour, it cannot model two stage nucleation (Vekilov, 2010), where solute molecules organize initially into an amorphous cluster, from which long range crystal order then emerges on cluster rearrangement. Despite these many limitations, CNT is useful to benchmark crystallization experiments because this approach has been so widely adopted. More importantly here, it allows useful insights into the crystallization process that are readily apparent due to its simplicity. In particular, the use of CNT has enabled us to establish that thermodynamic control of crystallization is possible in 3D nanoconfined volumes, as shown below.

2.1.1 Adoption of CNT to curved interfaces

For crystallization in nanodroplets, the planar substrate of CNT's heterogeneous nucleation formulation is replaced by a highly curved concave substrate. For such curved substrates, the free energy becomes (Cooper et al., 2008; Fletcher, 1958):

$$\Delta F_{het} = -\frac{4}{3v_c}\pi r^3 \Delta\mu[(f(\theta+\phi)-(R/r)^3 f(\phi)] + 2[1-\cos(\theta+\phi)]\pi r^2\gamma - 2\cos\theta(1-\cos\phi)\pi R^2\gamma \quad (6)$$

where θ is the contact angle between the nucleus and the spherical substrate, ϕ is the angle between the spherical substrate and the plane connecting the nucleus edge and $f(\alpha) = 0.25\left(2-3\cos\alpha+\cos^3\alpha\right)$ (see Figure 2a). Note that for concave surfaces, corresponding to crystallization within the curved substrate, R and ϕ are assigned negative values.

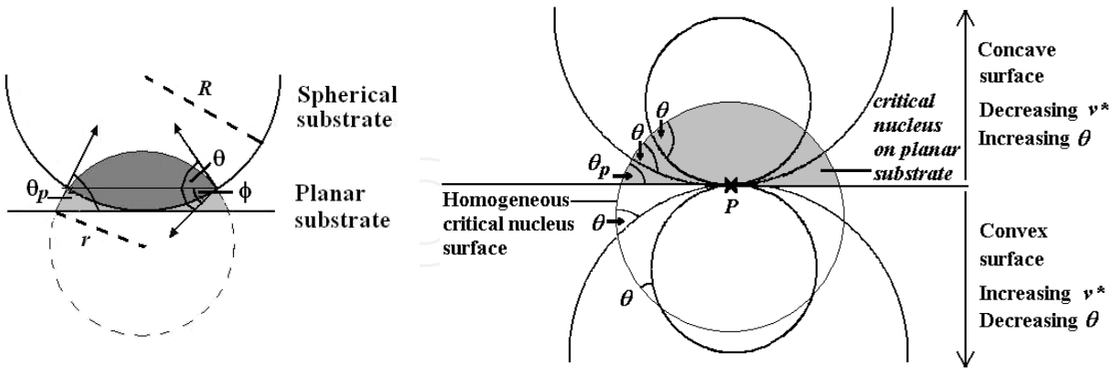
The maximum in ΔF_{het} gives the barrier to nucleation, ΔF^*_{het}, and again this condition is satisfied when $r^* = 2\gamma v_c / \Delta\mu$ to give:

$$\Delta F^*_{het} = \frac{\Delta F^*_{\text{hom}}}{2}\left\{1-3x^2\cos\theta+2x^3+y(1+x\cos\theta-2x^2)\right\} = \Delta F^*_{\text{hom}} f(\theta_p) \quad (7)$$

where $x = R/r^*$, $y = \pm\left(x^2-2x\cos\theta+1\right)^{0.5}$ with the positive and negative roots applying to a nucleus on a convex and concave surface, respectively and $\cos\theta_p = x - y$. θ_p is the angle between the corresponding planar critical nucleus and the plane tangential to the curved substrate surface, as shown in Figure 2a.

Equation (7) shows that at a given temperature, and hence constant ΔF^*_{hom} value, ΔF^*_{het} depends only upon the θ_p value. Consequently in Figure 2b, all the spherical substrates depicted result in the same ΔF^*_{het} value. This can be rationalized as follows. For nucleation on a concave surface, the critical nucleus volume, v^*, is reduced compared to the planar case, and hence fewer molecules need to cluster together to form the critical nucleus. However this effect is negated by the greater contact angle, θ, compared to θ_p, which means that more work is required to create unit area of the nucleus-substrate interface, and so the mean energy increase on addition of a molecule to the sub-critical nucleus is

larger. In contrast on a convex substrate, v^* is increased compared to the planar case, but θ is decreased.



(a) (b)

Fig. 2. (a) Schematic diagram describing nucleation upon a concave substrate of radius, R. The dark grey regions depict the nucleus on the concave surface. (b) Schematic diagram showing that for a given supersaturation, and hence critical nucleus radius, r^*, all surfaces through point P that cross the homogeneous critical nucleus surface produce the same ΔF^*_{het} value for nucleation, since they all have the same θ_p value (Cooper et al, 2008).

The onset temperature for the phase transition, e.g. the highest temperature, T_{trans}, at which crystallization should be observable, can then be found by setting the nucleation rate, J_{trans}, at T_{trans} to a suitable detection limit, where $J_{trans} = \Omega \exp\left(-\Delta F^*/kT_{trans}\right)$. The pre-exponential factor, Ω, can be considered constant provided the temperature range is narrow, since ΔF^* has the greater temperature dependence. Using $\left(\Delta F^*/k\right) = \left(T_{eq} - \Delta T_{trans}\right)\ln(\Omega / J_{trans})$, where $\Delta T_{trans} = T_{eq} - T_{trans}$, and substituting in equations (3), (5) and (7), gives:

$$\Delta T_{trans}{}^3 - \Delta T_{trans}{}^2 T_{eq} + \frac{16\pi\gamma^3 v_c{}^2 T_{eq}{}^2 f(\theta_p)}{3k\Delta_{fus}H^2 \ln\left(\Omega / J_{trans}\right)} = 0 \cdot \tag{8}$$

This equation has three roots corresponding to (1) The onset crystallization temperature T_c, (2) the expected onset melting temperature, T_m, for a nucleation-based melting transition, which would be required if surface melting did not occur, and (3) a non-physical root $T_c = \left(2T_{eq}/3\right)\{1-\cos W\}$ close to 0 K corresponding to the case where the critical nucleus contains only one molecule and the energy barrier is vanishingly small. T_c and T_m are given by:

$$T_{c,m} = \frac{T_{eq}}{3}\left\{2 + \cos W \mp (3^{0.5}\sin W)\right\} \tag{9}$$

where $W = \frac{1}{3}\arccos\left[1 - \frac{72\pi\gamma^3 v_c{}^2 f(\theta_p)}{k\Delta_{fus}H^2 T_{eq}\ln\left(\Omega / J_{trans}\right)}\right]$.

Hence T_c and T_m can be found with x, θ, T_{eq}, v_c, γ, $\Delta_{fus}H$ and Ω/J_{trans} as input. r^* and R can then be obtained from the Gibbs-Thomson equation, and $R = r^* x$, respectively.

From equation (7), we find that for a constant contact angle, θ, the energy barrier to nucleation is smaller for a concave surface than a convex one, and that the reduction in energy increases as $|x|$ increases. The onset crystallization temperatures, T_c, obtained from equation (9) are therefore correspondingly higher for concave surfaces. Figure 3 shows the expected T_c as a function of $|R|$ for the case of ice crystallization on a concave surface with a contact angle, θ, between the crystal nucleus and substrate of (a) 180°, i.e. the homogeneous nucleation case and (b) 100°. The onset melting temperatures, T_m, expected for the same systems (i.e. with supplementary contact angles between the melt-nucleus and substrate of (a) 0° and (b) 80°) in the absence of surface melting are also shown in this Figure. This melting is denoted nucleation-melting. The T_m and T_c curves meet at $|R_{min}|$ and at smaller concave radii, the melting curve falls below the crystallization one, which is clearly non-physical. Hence, equation (9) cannot model crystallization in 3D nanoconfinements smaller than $|R_{min}|$. This demonstrates a fundamental limitation of the theory, and shows that a key factor necessary for crystallization has been ignored.

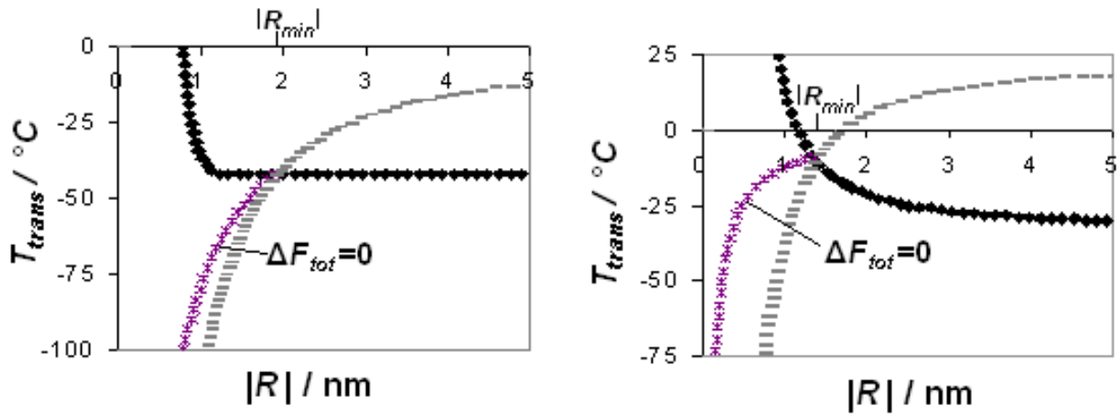


Fig. 3. The predicted ice onset crystallization temperatures, T_c, (filled diamonds) and nucleation-melting temperatures, T_m, (dashes), which would occur in the absence of surface melting, as a function of substrate radius, $|R|$, for crystallization within a spherical substrate with (a) θ = 180° and (b) θ=100°. The ice T_c have been determined using reasonable values (Pruppacher , 1995; Bartell , 1998; Speedy, 1987) of $v_c = 3.26 \times 10^{-29}$ m^3, $\gamma = 20$ mN m^{-1}, $\Delta_{fus}H = 4060$ J mol^{-1} and $\Omega/J_{trans} = 10^{18}$ for homogeneous nucleation and values of $v_c = 3.26 \times 10^{-29}$ m^3, $\gamma = 22$ mN m^{-1}, $\Delta_{fus}H = 5000$ J mol^{-1} and $\Omega/J_{trans} = 10^{15}$ for the heterogeneous nucleation case. Note that for $|R| < |R_{min}|$, the ice T_c and T_m are both given by the curve labelled $\Delta F_{tot} = 0$, as the transition temperature is now determined by the condition that the nucleus grows to a size r_0.

2.2 Phase transitions within nanoconfined volumes (Cooper et al., 2008)

2.2.1 Crystallization from the melt

The phase transition temperature in equation (9) is determined only by the ability to surmount the nucleation barrier. The thermodynamic feasibility of the transition, i.e. whether the new phase is stable with $\Delta F \leq 0$, however, is not considered. In fact, the crossing point of the crystallization and nucleation-melting curves, occurring at a droplet size

denoted R_{min}, corresponds to the system where the total phase transition of the droplet, from all liquid to all crystal, or vice versa, occurs with a free energy change $\Delta F_{tot} = 0$. For droplet sizes smaller than $|R_{min}|$, the nucleation-melting and crystallization curves describe systems where $\Delta F_{tot} > 0$, so the phase transformation would not proceed. This means that for sizes below $|R_{min}|$, the critical nucleus size can be attained as ΔF^*_{het} is surmountable, but there is then insufficient material within the confining substrate for ΔF to decrease to zero through further nucleus growth, e.g. in Figure 1a, the nucleus cannot grow to a size r_0. Consequently, below $|R_{min}|$ the crystallization and nucleation-melting curves must both follow the same curve labelled $\Delta F_{tot} = 0$ in the Figure to ensure a thermodynamically feasible phase transformation occurs. Hence the hysteresis normally observed upon heating and cooling the *same* system would be expected to disappear for phase transformations confined to within volumes with $|R| \leq |R_{min}|$. Unfortunately, there is a difficulty in verifying this lack of hysteresis experimentally, because this would require the r_0 nuclei to be constrained to this size. Typically, however, the r_0 nuclei subsequently grow via collisions with uncrystallized droplets, by oriented attachment of other nuclei, or by Ostwald ripening, and so it is difficult to ensure that subsequent melting and crystallization cycles are indeed performed on the same system.

Using the condition that for droplet sizes with $|R| \leq |R_{min}|$, $\Delta F_{tot}=0$ on complete crystallization of the spherical droplet, we find:

$$R = \frac{3v_c\gamma}{\Delta\mu}\cos\theta = \frac{3}{2}r^*\cos\theta \,. \tag{10}$$

Here we have retained the convention that the substrate radii, R, must take negative values for nucleation on a concave surface. Consequently, the critical nucleus size can be obtained from equation (10) if R and θ are known. This is an important finding because determination of r^* usually relies on the Gibbs-Thomson equation and the inappropriate application of bulk interfacial tension values to small nuclei. The number of molecules, n^*, in the critical nucleus is then given by:

$$n^* = \frac{v^*}{v_c} = \frac{4\pi|R|^3}{3v_c}\left\{\frac{1}{2} - \frac{4}{27\cos^3\theta}\left(1 - \frac{2-(3/4)\cos^2\theta + (9/8)\cos^4\theta}{\left(4-3\cos^2\theta\right)^{0.5}}\right)\right\}. \tag{11}$$

The dependence of n^* on θ is relatively weak, so that even if θ can only be estimated to within ~10%, n^* is known with good precision if R can be measured. For homogeneous nucleation (θ = 180°), equation (10) and (11) simplify to $r^* = 2|R|/3$ and $n^* = 32\pi|R|^3/81v_c$, so experimental measurement of R directly gives r^* and n^* provided $|R| \leq |R_{min}|$. So we just need to find the value of $|R_{min}|$.

An empirical determination of the R_{min} value is possible for homogeneous nucleation because the onset crystallization temperature, T_c, should be approximately constant for confinements with sizes above $|R_{min}|$. Note though that nucleation is a stochastic process, so repeated experiments will show some slight variation but an expected homogeneous nucleation temperature should nevertheless be apparent. For instance, the homogeneous nucleation temperature for ice is ≈-40 °C (Wood & Walton, 1970; Clausse et al., 1983).

Consequently, $|R_{min}|$ is readily identifiable as the droplet size at which T_c begins to decrease with decreasing $|R|$, provided the system nucleates homogeneously. For heterogeneous nucleation, θ is also likely to be a function of R, so an empirical determination is more difficult. Instead, the theoretical R_{min} value can be used, which is obtained as follows.

Substituting for r^* in equation (10) using the Gibbs-Thompson equation, $r^* = 2\gamma v_c / \Delta\mu = 2\gamma v_c T_{eq} / \Delta_{fus}H\Delta T_{trans}$, we find that for $|R| \le |R_{min}|$, T_c and T_m are given by:

$$T_c = T_m = T_{eq}\left[1 + \frac{3\gamma v_c \cos\theta}{|R|\Delta_{fus}H}\right]. \tag{12}$$

Equation (12) has previously been identified (Couchman & Jesser, 1977) as giving the minimum possible melting temperature of a small particle. Our analysis shows that it also gives the maximum possible freezing temperature of a confined object (Vanfleet & Mochel, 1995; Enustun et al., 1990). R_{min} is then readily obtained by substituting in equation (9), since the T_c and T_m curves from equation (9) meet at R_{min}. Hence:

$$R_{min} = \frac{9\gamma v_c \cos\theta}{\Delta_{fus}H\left\{1 - \cos W + \left(3^{0.5}\sin W\right)\right\}} \tag{13}$$

Finding reliable R_{min} values from equation (13) requires knowledge of θ, γ and $\Delta_{fus}H$, which is problematic since the use of bulk θ, γ and $\Delta_{fus}H$ values for such small systems is likely to introduce unquantifiable errors. Consequently, the preferred methodology is that of using homogeneously nucleating systems to identify $|R_{min}|$ from the confinement size below which the onset crystallization temperatures, T_c, start to decrease. Then critical nucleus sizes can be reliably found for all sizes below $|R_{min}|$ using $r^* = 2|R|/3$ and $n^* = 32\pi|R|^3/81v_c$. Fortunately, crystallization in microemulsions often proceeds via homogeneous nucleation, making these the system of choice.

2.2.2 Crystallization from nanoconfined solution

Our crystallization model can be extended to crystallization of solutes from nanoconfined solutions, though here the situation is complicated by the decrease in supersaturation that arises as the nucleus grows. In particular, by adopting a classical homogeneous nucleation approach for crystallization from an ideal solution in a spherical confining volume, V, the free energy change, ΔF, to produce a nuclei containing n molecules would be given by (Cooper et al., 2008; Reguera et al., 2003) :

$$\Delta F = -n\Delta\mu + \gamma A + NkT\left\{\ln\left(1 - \frac{v}{Vv_c c_0}\right) - \frac{1}{v_c c_0}\ln\left(1 - \frac{v}{V}\right)\right\} \tag{14}$$

where $\Delta\mu = kT\ln\left(c / c_{eq}\right)$ denotes the supersaturation at that nucleus size, with $c = (N-n)/(V-v) = c_0\left\{1 - \left(v/Vv_c c_0\right)\right\}\left\{1/\left(1 - v/V\right)\right\}$, γ and A denote the interfacial tension and surface area, respectively, at the nucleus-solution interface, N is the initial number of solute molecules when n = 0, v denotes the nucleus volume, v_c denotes the molecular

volume of the crystalline species and c_0 denotes the initial solute concentration when n = 0. The first two terms comprise those expected from classical nucleation theory for crystallization from unconfined volumes, whilst the third term provides the correction due to the supersaturation depletion as the nucleus grows. The free energy difference, ΔF, now exhibits a maximum, ΔF^*, corresponding to the critical nucleus radius, r^*, *and a minimum*, ΔF^*_{min}, at a larger nucleus radius, r^*_{min}, owing to the decrease in the supersaturation as the nucleus grows. r^* and r^*_{min} are both given by the usual Gibbs-Thomson equation with ΔF^* and ΔF^*_{min} both given by:

$$\Delta F^* = \frac{16\pi\gamma^3 v_c{}^2 T_{eq}{}^2 f(\theta_p)}{3\Delta_{fus}H^2\Delta T_c{}^2} + NkT\left\{\ln\left(1-\frac{v^*}{Vv_cc_0}\right)-\frac{1}{v_cc_0}\ln\left(1-\frac{v^*}{V}\right)\right\}, \tag{15}$$

where v^* denotes the nucleus volume when $r = r^*$, with the subscript *min* used to distinguish the minimum value from the maximum, and T_{eq} denotes the saturation temperature for the solution at concentration c^* surrounding the critical nucleus, r^*.

As before, the onset crystallization temperature is found from $\left(\Delta F^* / kT_c\right) = \ln(\Omega / J_{trans})$, with Ω assumed constant. This leads to a quartic equation (Cooper et al., 2008):

$$\Delta T_c{}^4 - T_{eq}\Delta T_c{}^3 + (X-Y)\Delta T_c + T_{eq}Y = 0 \tag{16}$$

where $X = \dfrac{16\pi\gamma^3 v_c{}^2 f\left(\theta_p\right)T_{eq}{}^2}{3k\ln\left(\Omega / J_{trans}\right)\Delta_{fus}H^2}$

and $Y = -\dfrac{32\pi c_0}{3\ln\left(\Omega / J_{trans}\right)}\left(\dfrac{\gamma v_c T_{eq}x}{\Delta_{fus}H}\right)^3\left\{\ln\left(1-\dfrac{v^*}{Vv_cc_0}\right)-\dfrac{1}{v_cc_0}\ln\left(1-\dfrac{v^*}{V}\right)\right\}$.

Equation (16) reduces to equation (8), the melt crystallization case, when Y = 0. Equation (16) is solvable with x, θ, c_0, T_{eq}, v_c, γ, $\Delta_{fus}H$ and Ω/J_{trans} as input. For the typical case where $T_c \le T_{eq}$, T_c is then given by:

$$T_c = \frac{3T_{eq}}{4} + z_1{}^{0.5} + z_2{}^{0.5} - z_3{}^{0.5} \tag{17}$$

where: $z_1 = \left\{-\left[\dfrac{T_{eq}\left(X+3Y\right)}{48}\right]^{0.5}\left(\cos\left(\dfrac{Z}{3}\right)-3^{0.5}\sin\left(\dfrac{Z}{3}\right)\right)\right\}+\dfrac{T_{eq}{}^2}{16}$,

$$z_2 = \left\{-\left[\frac{T_{eq}\left(X+3Y\right)}{48}\right]^{0.5}\left(\cos\left(\frac{Z}{3}\right)+3^{0.5}\sin\left(\frac{Z}{3}\right)\right)\right\}+\frac{T_{eq}{}^2}{16},$$

and

$$z_3 = \left\{\left[\frac{T_{eq}\left(X+3Y\right)}{12}\right]^{0.5}\cos\left(\frac{Z}{3}\right)\right\}+\frac{T_{eq}{}^2}{16},$$

where $Z = \arccos\left\{\frac{27^{0.5}\left[T_{eq}{}^{3}Y + (X-Y)^2\right]}{2\left[T_{eq}\left(X+3Y\right)\right]^{1.5}}\right\}$.

r^* and R are then found from the Gibbs-Thomson equation, and $R = r^* x$, respectively.

Of the other three solutions to the quartic equation (16), two are non-physical, as they correspond to either crystallization close to 0 K, or the onset crystallization temperature close to T_{eq} found when the minimum free energy radius, r^*_{min} , is used instead of the maximum value, r^*. The remaining solution provides the onset crystallization temperature for rare cases when $T_c > T_{eq}$, which could in principle arise for sufficiently soluble species when $\theta < 90°$. In this case, positive values of x are used since r is negative as well as R and

$$T_c = \frac{3T_{eq}}{4} + z_1{}^{0.5} - z_2{}^{0.5} + z_3{}^{0.5} . \tag{18}$$

As with the melt crystallization case, equations (17) and (18) are valid until the confinement size decreases to such an extent that there is insufficient crystallizing material present to ensure an energetically feasible phase transformation. For instance, crystallization would not be possible in a 3D-nanoconfined solution having the ΔF vs r curve shown in Figure 4a, since $\Delta F^*_{min} > 0$. For these small nanoconfinements, crystallization becomes feasible when the *minimum energy* ΔF^*_{min} is set to zero so that $r^*_{min} = r_0$, i.e. a stable nucleus can form. We then obtain (Cooper et al., 2008):

$$R = \frac{\gamma f(\theta_{p,min})}{kT_c c_0 x_{min}{}^2\left\{\ln\left(1-\frac{v^*_{min}}{Vv_c c_0}\right) - \frac{1}{v_c c_0}\ln\left(1-\frac{v^*_{min}}{V}\right)\right\}} = \frac{2\gamma v_c x_{min}}{kT_c \ln(c^*_{min}/c_{eq})} \tag{19}$$

from which:

$$x_{min} = \frac{R}{r^*_{min}} = \left(\frac{\ln(c^*_{min}/c_{eq}) f(\theta_{p,min})}{2v_c c_0 \ln\left(1-\frac{v^*_{min}}{Vv_c c_0}\right) - 2\ln\left(1-\frac{v^*_{min}}{V}\right)}\right)^{\frac{1}{3}} \tag{20}$$

where v^*_{min} denotes the volume of the r^*_{min} nucleus with ΔF = 0, $\partial\Delta F/\partial r = 0$, and $\partial^2\Delta F/\partial r^2 > 0$, and c^*_{min} denotes the solute concentration surrounding the r^*_{min} nucleus. Equation (20) can be solved iteratively to give $x_{min} = R/r^*_{min}$ with inputted values for c_0, θ, v_c and c_{eq}, but again, crucially not the γ or $\Delta_{fus}H$ values. The x value is then given by:

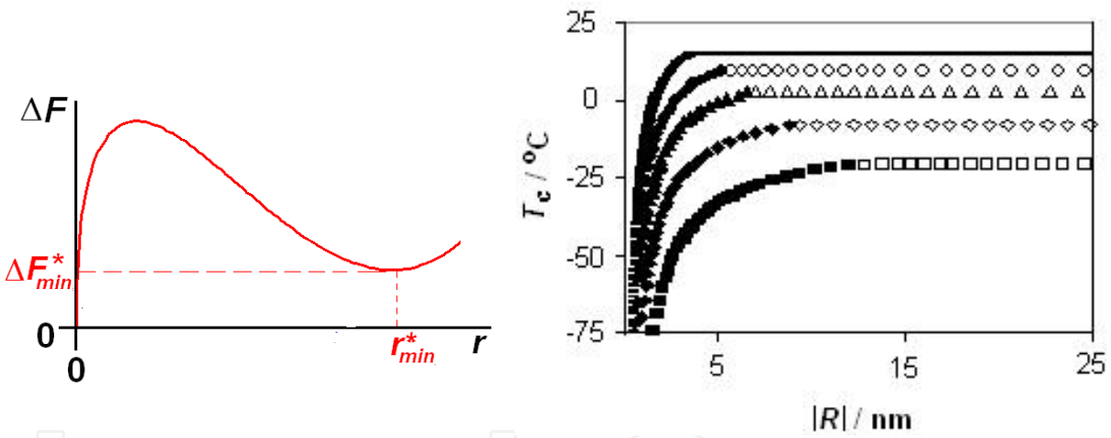
$$\frac{x}{\ln(c^*/c_{eq})} = \frac{x_{min}}{\ln(c^*_{min}/c_{eq})} . \tag{21}$$

Thus we can work out $r^* = R/x$ just by measuring R and T_c values, when $|R| \leq |R_{min}|$. The number of molecules, n^* $(= v^*/v_c)$ in the critical nucleus is also obtained from R, θ, c_0, v_c, and T_c as input and is given by:

$$n^* = \frac{4\pi R^3}{3v_c x^3}\left\{\frac{1}{2} - \frac{x^3}{2} + \frac{2 - 2x\cos\theta + x^2 - x^2\cos^2\theta - 2x^3\cos\theta + 2x^4}{4y}\right\}, \quad (22)$$

which for homogeneous nucleation (θ = 180°, $y = x + 1$) reduces to the expected $n^* = 4\pi r^{*3}/3v_c$.

Hence provided $|R| \leq |R_{min}|$, we can again determine both n^* and r^* without reliance on macroscopic γ and $\Delta_{fus}H$ values, provided we know or can estimate θ. The experimental onset crystallization temperature, T_c, can then be compared with the values predicted from the Gibbs-Thomson and ideal solubility equations using the experimentally found R, x, and c_{eq} values. This provides a measure of how bulk values of γ and $\Delta_{fus}H$ are likely to be perturbed for solute crystallization in nanosystems. Figure 4a shows a schematic graph of ΔF vs r, whist Figure 4b shows theoretical calculations using equations (17) and (19) to model the homogeneous nucleation of octadecane from dodecane solutions, illustrating again the decrease in T_c that occurs below $|R_{min}|$, from which the critical nucleus size can be estimated.



(a) (b)

Fig. 4. (a) Schematic graph of ΔF vs r for crystallization in a 3D-nanoconfined solution. (b) Graph showing T_c, with confinement radius, $|R|$, for homogeneous nucleation from solutions of octadecane in dodecane. Open symbols correspond to the regime where $\Delta F^* = kT_c \ln(\Omega / J_{trans})$ gives T_c, filled symbols to the regime where $|R| \leq |R_{min}|$ and T_c is controlled by $\Delta F^*_{min} = 0$. Squares = 0.1 mole fraction of octadecane in dodecane, diamonds = 0.25 mole fraction, triangles = 0.5 mole fraction and circles = 0.75 mole fraction. The uppermost curve corresponds to the pure octadecane liquid case, with the thicker line portion showing the regime controlled by $\Delta F_{tot} = 0$ (Cooper et al., 2008).

2.2.3 Thermodynamic control of crystallization

The above analysis show that for all confinement sizes below $|R_{min}|$, crystallization is not governed by the ability to surmount the nucleation barrier, ΔF^*, but by the ability to create a

thermodynamically feasible new phase , i.e. $\Delta_{tot}F \leq 0$ for melt crystallization or $\Delta F^{*}_{min} \leq 0$ for solution crystallization. This means that crystallization is under thermodynamic, rather than the usual kinetic, control. This is significant because crystallization can then be directed to generically produce the most stable crystalline phase in 3D nanoconfined solutions and liquids. This finding is particularly important for polymorphic compounds.

3. Polymorphism

Polymorphism occurs when a substance can crystallize into more than one crystal structure. Each polymorph of a substance will have differing physical properties e.g. melting points, solubilities, compaction behaviour etc. In the pharmaceutical industry, it is imperative that a drug does not transform post-marketing, as this can affect its bioavailability, and reduce the drug's effectiveness. An infamous example of this occurred for the anti-HIV drug, Ritonavir (Chemburkar et al., 2000). In 1998, 2 years after marketing the drug in the form of soft gelatine capsules and oral solutions, the drug failed dissolution tests; a less soluble, thermodynamically more stable, polymorph had formed. This resulted in the precipitation of the drug and a marked decrease in the dissolution rate of the marketed formulations, reducing its bioavailability. Consequently Ritonavir had to be withdrawn from the market and reformulated, to the cost of several hundred million dollars.

The Ritonavir case highlights that crystallization is typically under kinetic control, with metastable polymorphs often crystallizing initially in accordance with Ostwald's rule of stages (Ostwald, 1897). For pharmaceutical companies, Ostwald's rule is a nemesis, as it means that their strategy of relying on high throughput screening of different crystallization conditions in order to identify stable polymorphs is scientifically flawed and so may not succeed. Consequently the industry remains vulnerable to another Ritonavir-type crisis. If the crystallization can be conducted from 3D-nanoconfined solutions, however, the crystallization can be exerted under thermodynamic control so that the thermodynamically stable polymorph is crystallized directly. In particular, in Figure 5a it is evident that neither polymorph A in red or polymorph B in blue will crystallize from the nanoconfined solution,

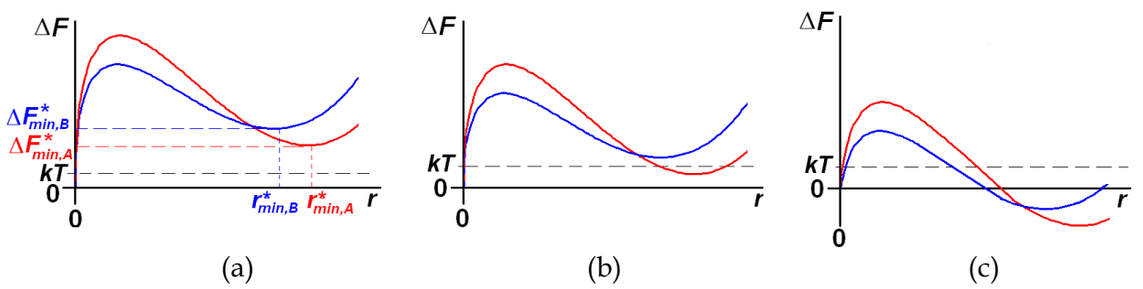


Fig. 5. Example graphs of free energy change, ΔF *vs.* nucleus size, r for crystallization of a polymorphic system from 3D nanoconfined solutions of monodisperse size and supersaturation. (a) System stabilized due to 3D nanoconfinement, with no observable crystallization. (b) Crystallization is under thermodynamic control with stable polymorph A (red) crystallizing, even though it has the higher nucleation barrier. (c) Crystallization occurs under kinetic control with metastable polymorph B (blue) as the majority product.

since for both $\Delta F^*_{\min} > kT$. In Figure 5b, however, polymorph A can form because it can produce a stable nucleus ($\Delta F^*_{min,A} < 0$) whereas polymorph B cannot. Hence provided the nucleation barrier is surmountable, this system will crystallize under thermodynamic control to directly give the stable polymorph A. In the system shown in Figure 5c, however, both polymorph A and B can form stable nuclei; crystallization will tend to be under kinetic control with polymorph B forming at a faster rate due to its lower nucleation energy barrier. Thus metastable B becomes the majority product in this case.

The thermodynamic arguments stated above are valid in the thermodynamic limit, where the system is so large that fluctuations do not significantly contribute to the equilibrium properties of the system. Though, of course, it must be remembered that it is these very fluctuations that enable critical nuclei to form and hence initiate the phase transformation. Consequently, in a system comprising a limited number of nanoconfined solutions, the fluctuations do need to be included to accurately model the equilibrium properties of the system (Reguera et al., 2003). We neglect this statistical thermodynamic description in our simple model of onset crystallization temperatures because the system in which we apply it, namely microemulsions, typically consists of a sufficiently large number of droplets, ~10^{18} per gram of microemulsion, which makes its additional complexity unwarranted. Moreover our simple model contains the essential features required to show how reliable estimates of critical nucleus sizes and thermodynamic control of crystallization are realizable in microemulsions.

4. Microemulsions

Microemulsions are thermodynamically stable, transparent mixtures of immiscible liquids. Typically they comprise oil droplets in water (an oil-in-water microemulsion) or water droplets in oil (a water-in-oil microemulsion). Bicontinuous microemulsions are also possible, however the absence of a 3D nanoconfined solution in these systems make them less suitable for thermodynamic control of crystallization. In the droplet microemulsions, the droplet size is typically 2-10 nm, with a relatively narrow polydispersity of σ_R/R_{max} ≈ 0.1-0.2, where σ_R is the Gaussian distribution standard deviation and R_{max} is the modal droplet radius (Eriksson and Ljunggren, 1995). The droplets are stabilized by surfactants, frequently in combination with a co-surfactant, which reside at the droplet interface, reducing the interfacial tension there to ~10^{-3} mN m^{-1}. This ultralow interfacial tension provides the thermodynamic stability of microemulsions, since the small free energy increase involved in creating the droplet interface is more than offset by the increased entropy of the dispersed phase. Note that this ultralow interfacial tension also ensures that the LaPlace pressure difference, $\Delta P = 2\gamma/R$, across the highly curved droplets is small. When the volume fraction of the dispersed phase becomes so low that its properties differ measurably from its usual bulk properties, the terms "swollen micelles", "swollen micellar solutions", "solubilized micellar solutions" or even simply "micellar solutions" can be used instead of microemulsions for oil-in-water systems, whilst for water-in-oil systems, the same terms but with "inverse" or "reverse" inserted before "micelle" or "micellar" may be used. However, because there is, in general, no sharp transition from a microemulsion containing an isotropic core of

dispersed phase and a micelle progressively swollen with the dispersed phase, many researchers use the term "microemulsion" to include swollen micelles (or swollen inverse micelles) but not micelles containing no dispersed phase. This is the context in which the term "microemulsion" is used here. In the microemulsions, dissolved solutes may be supersaturated within the discontinuous (dispersed) phase, or the dispersed liquid may be supercooled, so that crystallization in the microemulsions can occur. The solute molecules are assumed to be distributed amongst the microemulsion droplets with a Poisson distribution, so that most droplets will have a supersaturation close to the mean, but a minority will have supersaturations significantly higher than the mean.

Microemulsions are dynamic systems with frequent collisions occurring between the droplets. The most energetic of these collisions cause transient dimers to form, allowing the exchange of interior content between the droplets. This exchange means that microemulsions can act as nanoreactors for creating quantum dots and other inorganic nanoparticles, for example. A recent review (Ganguli et al., 2010) on inorganic nanoparticle formation in microemulsions highlights the progress that has been made in this area from its inception with metal nanoparticle synthesis in 1982 by Boutonnet et al., followed by its use in synthesizing quantum dots (Petit et al. 1990) and metal oxides (see e.g. Zarur & Ying, 2000). The transient dimer mechanism also enables crystallization to proceed in microemulsions whenever a transient dimer forms between a droplet containing a crystal nucleus and a nucleus-free droplet which contains supersaturated solution, since the crystal nucleus can then gain access to this supersaturated solution and thereby grow (see Figure 6). Crystallization of organic compounds from microemulsions was first studied by Füredi-Milhofer et al. in 1999 for the aspartame crystal system, with studies on glycine crystallization (Allen et al., 2002; Yano et al., 2000; Nicholson et al., 2011; Chen et al., 2011) and carbamazepine (Kogan et al., 2007) following. The use of microemulsions in producing both inorganic nanoparticles and macroscopic organic crystals shows that the size of the particulates grown can vary from a few nm to mm, depending upon the nucleation rate, the ability to form stable nuclei, and the extent of surfactant adsorption on the resulting particles. Our interest in microemulsions stems from their intrinsic ability to enable reliable estimates of critical nucleus sizes and to exert generic thermodynamic control over the crystallization process for the first time.

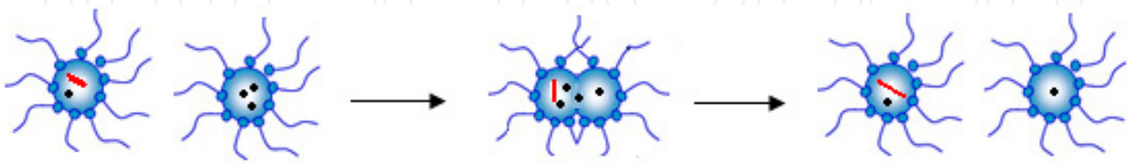


Fig. 6. Schematic diagram illustrating an energetic collision between a microemulsion droplet containing a crystal nucleus and a nucleus-free droplet containing supersaturated solution. The energetic collision results in a transient dimer forming, enabling the nucleus to gain access to more molecules and grow. The crystal nucleus is shown in red and the solute molecules are shown in black. The surfactant molecules stabilizing the microemulsion droplets are depicted as blue circles with tails.

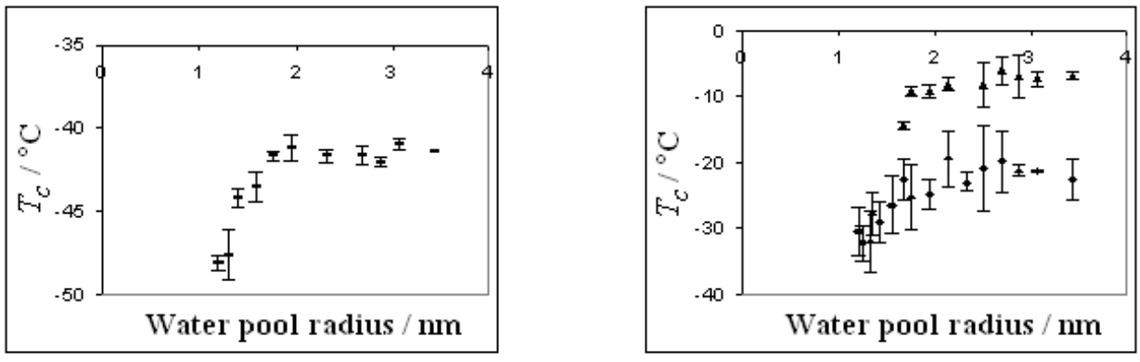
4.1 Measurement of the critical nucleus size in microemulsions

Reliable estimates for the critical nucleus size can be found for homogeneous nucleation in microemulsions. The homogeneous nucleation temperature should be approximately constant until the droplet size decreases to below $|R_{min}|$, and thereafter the temperature should decrease. In the region where T_c decreases, the crystallization is controlled by the requirement that $\Delta_{tot}F \leq 0$, rather than the size of the nucleation energy barrier. Consequently, the critical nucleus size can be estimated by measuring the droplet size $|R|$ and assuming a spherical nucleus so that $r^* = 2|R|/3$ and $n^* = 32\pi|R|^3/81v_c$. Whilst homogeneous nucleation is comparatively rare in bulk systems, in microemulsions it is more prevalent for two main reasons. Firstly, the droplets are too small to contain foreign material onto whose surfaces heterogeneous nucleation could arise. Secondly, the ability of the surfactants to induce heterogeneous nucleation is often reduced in microemulsions compared to that at planar interfaces and in emulsions, particularly for crystallization from solution. This is because nuclei formation on the surfactant layer is disfavoured at this ultra low interfacial tension interface, and the high curvature may also hinder any templating mechanism that operates at more planar interfaces. The reduction in adsorption is readily apparent from Young's equation, $\cos\theta = (\gamma_1 - \gamma_2)/\gamma$ where θ is the contact angle, γ is the interfacial tension between the crystallizing species and the surrounding melt/solution, with γ_1 and γ_2 denoting the interfacial tensions between the surfactant and immiscible phases, and the surfactant and crystallizing species, respectively. The lowering of γ_1 that occurs in going from an emulsion to a microemulsion results in a higher contact angle, θ, and hence reduced adsorption for the crystallizing species.

Given this, we might expect heterogeneous nucleation to be impeded in microemulsions, and indeed other systems with low interfacial tensions, γ_1. Such an effect was observed at the phase inversion of an emulsion using Span 80 and Tween 80 surfactants to induce β-glycine crystallization at the oil-aqueous interface (Nicholson et al., 2005). Similarly, the ability of the nonionic surfactants, Span 80 and Brij 30 to heterogeneously nucleate glycine was negligible in microemulsions containing these mixed surfactants (Chen et al., 2011), whereas they promoted the metastable β-glycine nucleation at planar interfaces and in emulsions (Allen et al., 2002; Nicholson et al., 2005). There are literature examples where nonionic surfactants do induce heterogeneous nucleation in microemulsions, though. For instance, ice nucleation was promoted by adding heptacosanol, a long chain alcohol cosurfactant, to AOT microemulsions (Liu et al., 2007). Long chain alcohols can induce ice nucleation at temperatures of ≈-2 °C at planar air-water interfaces (Popovitz-Biro et al., 1994) and at ≈-8 °C at emulsion interfaces (Jamieson et al., 2005). This nucleating ability was diminished in the microemulsions. Nevertheless, ice crystallization still tended to occur at temperatures in the range of ≈-9 to -30 °C depending upon the heptacosanol concentration in the microemulsion droplets (Liu et al., 2007), i.e. much higher than the homogeneous nucleation temperature of ≈-40 °C (Wood & Walton, 1970; Clausse et al., 1983). For ionic surfactants, like AOT, heterogeneous nucleation in microemulsions can also occur. The longer range electrostatic interactions of ionic surfactants can induce order without requiring direct adsorption onto the surfactant layer. It is important, therefore, to choose surfactants that do not promote crystallization when placed at the planar air-liquid

or air-solution interface to ensure that homogeneous nucleation occurs in the microemulsions.

Once a suitable homogeneous nucleating microemulsion system has been found, the onset crystallization temperature, T_c, for microemulsions of varying size, R, can be found by a suitable technique, such as differential scanning calorimetry (DSC). It can be assumed that the exothermic DSC peak arising from the crystallization of the droplets corresponds to the temperature range in which the majority of droplets can crystallize, so that the mean droplet size can be used to accurately determine r^* and n^*. The mean droplet size of the microemulsion can be determined from small angle X-ray scattering, or small angle neutron scattering measurements. This methodology allows a simple and accurate measurement of the critical nucleus size, and is particularly useful for crystallization of liquids, or solutes which have a high solubility in the confined phase, so that there is sufficient crystallizable material present within the microemulsion for the exothermic crystallization peak to be observable by DSC. We have recently applied this methodology to ice crystallization in AOT microemulsions (Liu et al., 2007). Figure 7a shows homogeneous ice nucleation in AOT microemulsions, compared to heterogeneous nucleation in Figure 7b where the cosurfactant heptacosanol is added to the AOT microemulsions. The larger error bars in the heterogeneous nucleation case shown in Figure 7b reflect the varying number of heptacosanol molecules in the droplets that cause ice nucleation. For the homogeneous case, the reduction in T_c with $|R|$ occurs at $|R_{min}| \approx 2$ nm in Figure 7a, in good agreement with the theoretical value shown in Figure 3a. From this, the critical nucleus at R_{min} can be estimated to contain ≈280 molecules (Liu et al., 2007).



(a) (b)

Fig. 7. Variation of observed ice onset crystallization temperatures, T_c, with water pool size for microemulsions with (a) AOT and (b) AOT plus heptacosanol The error bars show the standard deviation from three or more measurements. The nucleation is homogeneous in (a) and heterogeneous in (b). In the AOT microemulsions with added heptacosanol, several crystallization peaks were often evident, due to the droplets having differing numbers of the heptacosanol cosurfactant molecules that help nucleate ice. Consequently in (b) the highest T_c peak (upper curve) and largest T_c peak (lower curve) are just plotted for clarity (Liu et al. 2007).

4.2 Thermodynamic control of crystallization in microemulsions: Leapfrogging Ostwald's rule of stages

As detailed previously, crystallization within 3D nanoconfined solutions differs fundamentally from bulk crystallization because the limited amount of material within a nanoconfined solution results in the supersaturation decreasing substantially as the nucleus grows, leading to a minimum[11,12] in the free energy, $\Delta F^*_{\min}$, at a post-critical nanometre nucleus size, $r^*_{\min}$ (see Figure 4a). This fact, in particular, allows stable polymorphs to be solution-crystallized from microemulsions even when they have high nucleation barriers. Hence thermodynamic control of crystallization can be generically achieved for the first time. Note that microemulsions differ in two main ways from the theoretical nanoconfined solutions considered previously in sections 2 and 3. Firstly, transient droplet dimer formation enables the nuclei to grow beyond that dictated by the original droplet size; in fact crystals ranging from nm to mm can be produced. Secondly, microemulsions are polydisperse. There will be a range of droplet sizes and supersaturations in any microemulsion system, which must be considered to enable thermodynamic control of crystallization. An effective strategy is detailed below.

The equilibrium population of the $r^*_{\min}$ nuclei in the microemulsion depends upon the Boltzmann factor, $\exp\left(-\Delta F^*_{\min} / kT\right)$. Consequently, if $\Delta F^*_{\min} > kT$, the equilibrium population of the $r^*_{\min}$ nuclei will be very low. In contrast, if the $r^*_{\min}$ nuclei have free energies, $\Delta F^*_{\min} < kT$, they will have a sizeable equilibrium population. We term such $r^*_{\min}$ nuclei, (near) stable nuclei. Crystallization in microemulsions proceeds initially via the 3D nanoconfined nuclei gaining access to more material and growing during the energetic droplet collisions that allow transient dimers to form. *This crystallization process will be severely hindered if the population of such* $r^*_{\min}$ *nuclei is so low* as for the case depicted in Figure 5a, that the colliding droplets are highly unlikely to contain nuclei. In this case, the supersaturated system is stabilized due to the 3D nanoconfinement. In contrast, the crystallization can proceed readily via this transient droplet dimer mechanism if $\Delta F^*_{\min} < kT$

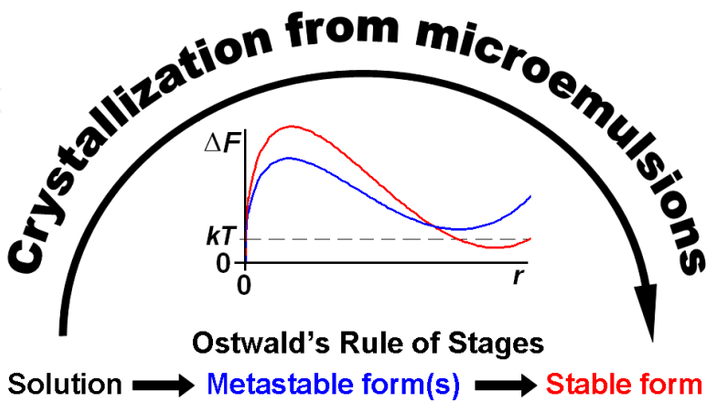


Fig. 8. A schematic diagram showing how Ostwald's rule of stages can be 'leapfrogged' by crystallizing from microemulsions. Stable polymorph A is in red, and metastable B is in blue. The ΔF vs r plot corresponds to the case where crystallization is brought under thermodynamic control so that stable polymorph A crystallizes directly.

because then a sizeable population of droplets will contain a (near) stable nucleus. *Thus, crystallization in microemulsions is governed by the ability to form (near) stable nuclei rather than critical nuclei.* In particular, recalling that there will be a range of droplet sizes and solute concentrations within the microemulsion droplets, thermodynamic control of crystallization can be achieved using the following methodology. The supersaturation in a microemulsion can be increased from one that is stabilized due to 3D nanoconfinement until the following condition is met: only the largest and highest supersaturation droplets, which contain the most material, can form (near) stable nuclei of only the most stable crystal form or polymorph. This situation is exemplified in Figure 8 with $\Delta F^*_{\min,A} \leq kT$ but $\Delta F^*_{\min,B} > kT$. Crystallization is then only just possible, and importantly, only the most stable polymorph will crystallize, as this is the only form for which (near) stable nuclei are likely to exist and so grow during transient droplet dimer formation. This generic strategy allows us to 'leapfrog' Ostwald's rule of stages and crystallize stable polymorphs directly.

The strategy detailed above will work provided $\Delta F^*_{\min,A} < \Delta F^*_{\min,B}$, and (near) equilibrium populations of the $r^*_{\min}$ nuclei are obtained. $\Delta F^*_{\min,A} < \Delta F^*_{\min,B}$ will typically be true because the stable polymorph has the greater bulk stability and it is the least soluble. Hence $r^*_{\min,A} > r^*_{\min,B}$ as stable polymorph *A* can grow to larger nucleus sizes, with typically lower free energies, than metastable *B* before its supersaturation is depleted. Equilibrium populations of the $r^*_{\min}$ nuclei will arise provided the $r^*_{\min}$ nuclei formation and dissolution processes are sufficiently rapid. This depends upon the magnitude of the nucleation barriers, ΔF^*, and the dissolution energy barriers, ΔF^* - $\Delta F^*_{\min}$, respectively. It can be ensured that the nucleation barriers to all polymorphs are surmountable by crystallizing from sufficiently small droplets. This is because the substantial supersaturation depletion that arises in a small droplet as the nucleus grows means that very high initial supersaturations with respect to the most stable polymorph are required to enable a (near) stable nuclei to form. Consequently it can reliably be assumed that the initial solutions in these droplets will also be sufficiently supersaturated with respect to all polymorphs that all nucleation barriers are indeed surmountable. The nuclei dissolution barriers, i.e. $\Delta F^* - \Delta F^*_{\min}$, will be surmountable when the ΔF^* barriers are surmounted and $\Delta F^*_{\min} \geq 0$ as in Figure 8, since then ΔF^* - $\Delta F^*_{\min} \leq \Delta F^*$. Hence thermodynamic control will indeed be obtainable if the largest and highest supersaturation droplets have free energy curves corresponding to Figure 8. Ostwald's rule will have been 'leapfrogged' because the high initial supersaturations ensure the nucleation barriers are 'leapt over' to directly give the most stable polymorph. In contrast, the analogous unconfined bulk system would crystallize the metastable polymorph initially, in accordance with Ostwald's rule, owing to its lower nucleation barrier.

Note that the ability of microemulsions to exert thermodynamic control over crystallization is independent of the nucleation path; it depends solely upon the ability to form (near) stable nuclei, rather than their formation pathway. Consequently this ability is generic, applying equally to systems that nucleate via a classical one stage mechanism, and to those where two stages are implicated.

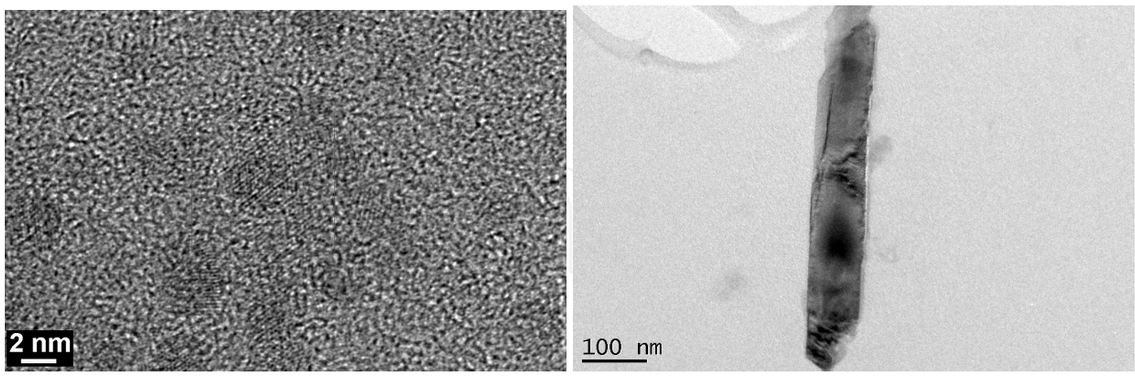
Once formed, the (near) stable nuclei can grow via transient droplet dimer formation until the nuclei become larger than the droplets or the supersaturation is relieved. For crystallites

larger than the droplets, subsequent growth can then occur via the following processes; energetic collisions with droplets that allow access to the droplets' interior contents, oriented attachment of other nuclei, and impingement from the (typically minuscule) concentration of their molecules in the continuous phase. Thus, the final crystal size can vary from nm to mm, depending upon the concentration of (near) stable nuclei, the supersaturation and the extent to which surfactant adsorption on the crystallites limits their growth rate.

In order to test the ability of microemulsions to exert thermodynamic control over crystallization, we chose three problem systems that had well-documented difficulty in obtaining their stable polymorphs: namely glycine, mefenamic acid and ROY (Nicholson et al., 2011). In each case, it was successfully demonstrated that the stable polymorph crystallized directly from the microemulsions under conditions where crystallization was only just possible. The time-scale at which ~mm sized crystals grew ranged from minutes to months. Solvent-mediated transformations to more stable polymorphs can occur in this timeframe, although such transformations would be expected to have a significantly reduced rate in microemulsions owing to the exceedingly low concentration of the polymorph's molecules in the continuous phase. Accordingly, transmission electron microscopy (TEM) was used to show that the nanocrystals crystallized within the first 24 hours in the microemulsions were also of the stable form, thereby proving that the initial crystallization was indeed in this form. TEM was performed on the microemulsions by dropping small aliquots of the microemulsions onto TEM grids, allowing the drops to (mostly) evaporate, and then washing the grids with the microemulsion continuous phase to remove residual surfactant. This left predominantly just the crystallites grown in the microemulsion droplets on the TEM grids. Figure 9 shows TEM images of stable Form I nanocrystals of mefenamic acid grown within 1 day from DMF microemulsions at 8 °C containing 80 mg/ml of mefenamic acid in the DMF (Nicholson & Cooper, 2011).

With increasing supersaturation, metastable polymorphs also crystallized from the microemulsions. The relative supersaturation increase that led to the emergence of metastable forms was highly system dependant, though. For instance, for glycine the stable γ-polymorph crystallized as the majority polymorph under mean initial supersaturation ratios of 2.0 to 2.3, for mefenamic acid the corresponding range was 4.1 to 5.3, whereas for ROY a much larger range of ≈10 to 24 was found. The small supersaturation range in which the stable γ-glycine polymorph crystallized as the majority form reflected the small relative energy difference of 0.2 kJ mol between the γ- and α-polymorphs and the much faster growth rate (~500 times) of the α-polymorph in aqueous solutions (Chew et al., 2007). Recall that when crystallization is only just possible in the microemulsions, the formation of (near) stable nuclei will be confined to only the largest droplets with the highest supersaturations. Hence the actual initial supersaturations that are required for crystallization to be just possible are always much higher than the mean initial values. An estimate of this actual initial supersaturation was found in the glycine system as follows. Assuming a Poisson distribution of solute molecules amongst the droplets, then for the glycine system, $<10^{-8}$ of the droplets formed (near) stable nuclei under conditions where crystallization was only just possible, since the 0.2 kJ mol^{-1} stability difference between the γ- and α-forms would only lead to thermodynamic preference for the stable γ-form if the (near) stable nuclei contained ~20-30 molecules (Nicholson et al., 2011). This meant initial supersaturation ratios of ~11-15

were necessary for crystallization to be possible in the glycine system. A similar analysis for the mefenamic acid case gives initial supersaturation ratios >15 (Nicholson & Cooper, 2011).



(a) (b)

Fig. 9. TEM images of stable Form I nanocrystals of mefenamic acid grown from DMF microemulsions. (a) ~4 nm nanocrystals grown in 12 hours and (b) a Form I nanocrystal grown in 24 hours.

These very high initial supersaturation ratios highlight two key factors governing the solution crystallization of stable polymorphs from microemulsions. Firstly, the substantial supersaturation decrease as a nucleus grows in a droplet means that very high initial supersaturations are needed for a (near) stable nucleus to form. Secondly, these very high initial supersaturations help ensure that the nucleation barriers to all possible polymorphs are surmountable. Hence, the use of microemulsions is the only way to crystallize a stable polymorph that has a very high nucleation barrier in bulk solution.

4.3 Practical considerations for choosing microemulsion systems

In choosing suitable microemulsion systems for achieving thermodynamic control of crystallization to obtain stable polymorphs, or for obtaining reliable estimates of critical nucleus sizes, the following should be considered.

1. The material to be crystallized should be insoluble, or only sparingly soluble in the microemulsion continuous phase. Since the material will have the same chemical potential at equilibrium in the continuous phase, as in the confined phase, the supersaturated material could potentially crystallize in the continuous phase with attendant loss of thermodynamic control. If the crystallizing material has a very low/negligible solubility in the continuous phase, however, the impingement rate onto a nucleus in this phase is so low that the nucleation rate and subsequent growth of such nuclei will be minimized. Then it can be reliably assumed that the crystallization is initially confined to the dispersed phase so that thermodynamic control is possible.
2. The nucleation should ideally be homogeneous. Choosing surfactants that do not promote crystallization at planar or emulsion interfaces helps ensure this. Homogeneous nucleation enables critical nucleus sizes to be obtained more reliably, since the contact angle of 180° is, of course, invariant with droplet size, R, and the relationships $r^* = 2|R|/3$ and $n^* = 32\pi|R|^3/81v_c$ are valid for droplet sizes

$|R| \leq |R_{\min}|$, i.e. where T_c decreases with $|R|$. Homogeneous nucleation is also preferred when aiming to crystallize stable polymorphs, since heterogeneous nucleation could potentially lead to a metastable polymorph having a lower $\Delta F^*_{\min}$ than the stable one, and thereby crystallizing in preference to the stable form.

3. Given that a metastable polymorph can potentially have the lowest $\Delta F^*_{\min}$ in a microemulsion if, for example, it is heterogeneously nucleated by the surfactant, or it is sufficiently stabilized by the surrounding solvent, or an inversion of stability between polymorphs occurs at nm sizes, then this possibility should be checked. This can be done readily by using a different solvent and/or surfactant. In addition, the supersaturation of the microemulsion should be gradually increased from the point at which crystallization is only just possible, until crystals/nanocrystals of more than one polymorph crystallize. In this way, all low energy polymorphs can be identified.
4. The crystallizable species, or more often the solvent, may be absorbed in the surfactant interfacial layer and so the solute concentration within the interior pool of the microemulsion droplet may differ substantially from the bulk concentration used in making the microemulsion. This possibility must be checked by measuring the solubility of the crystallizing species in the microemulsion, and then determining the mean initial supersaturation ratios accordingly. Accurate solubility measurements require adding powdered material to a microemulsion and leaving for a prolonged period (weeks) to ensure equilibration.
5. Bicontinuous and percolating microemulsions are not suitable systems for determining critical nucleus sizes or obtaining thermodynamic control of crystallization. In bicontinuous microemulsions, the absence of 3D nanoconfinement precludes their use. In percolating microemulsions, the droplets cluster and transiently form much larger droplets in which (near) stable nuclei of metastable polymorphs can form and grow, alongside the (near) stable nuclei of the stable form in the non-clustering droplets. For water-in-oil microemulsions, the absence of percolation and bicontinuous structures can be assumed if the microemulsions show minimal conductivity.
6. Microemulsions are thermodynamically stable and so form spontaneously upon mixing the constituents. Hence shaking by hand and vortexing are suitable preparation methods. Prolonged sonication should be avoided in case this affects the crystallization.
7. When the supersaturation in the microemulsions is achieved via anti-solvent addition or by a chemical reaction, a mixed microemulsion method should generally be implemented whereby two microemulsions are prepared. A different reactant is in each microemulsion, or for the antisolvent crystallization method, one microemulsion contains the undersaturated crystallizable species in a good solvent and the other microemulsion contains the antisolvent. On mixing the two microemulsions, transient dimer formation between droplets containing different reactants and/or solvents enables a relatively rapid equilibration of interior droplet content to take place, on the timescale of ~μs to ms (Ganguli et al., 2010). After this, it can be assumed that the dispersed reactants and solvents are distributed amongst the droplets with a Poisson distribution. Adding the antisolvent or second reactant drop-wise to the microemulsion should be avoided as this can create high concentration fluctuations immediately after the addition (Chen et al., 2011). Alternatively, if one of the reactants is soluble in the continuous phase, a solution of this reactant should be added to the microemulsion

containing the second reactant. Here, it is necessary to ensure the reaction proceeds predominantly in the microemulsion droplet, or at the droplet interface, by making sure that the second reactant has a negligible solubility in the continuous phase, whilst the first reactant must be able to partition into the droplet interface and/or interior.

8. For determining critical nucleus sizes, crystallization of liquids or high concentration solutes are preferred so that crystallization peaks are observable in the DSC. The crystallization peak is then associated with the mean droplet size $|\overline{R}|$, since close to this peak most droplets can form stable nuclei and crystallize. To obtain stable polymorphs, solution-crystallization from microemulsions is preferred, as then the substantial supersaturation decrease as the nuclei grow means that large initial supersaturations are required in order to create (near) stable nuclei and these help ensure the nucleation barriers to all polymorphs are surmountable. To ensure crystallization of stable polymorphs from microemulsions, the crystallization should only just be possible, so that the (near) stable nuclei only form in the largest droplets with the highest supersaturations. Hence the initial supersaturations and number of solute molecules in these droplets will be significantly higher than the mean values.

4.4 Crystallization of inorganic systems in microemulsions

Recently we have extended the thermodynamic control of crystallization methodology to inorganic polymorphic systems. There is much literature detailing inorganic nanoparticle formation via the mixed microemulsion approach (Ganguli et al, 2010). However, often the nanoparticles obtained are amorphous and so require high temperature and/or high pressures to introduce crystallinity. For instance, many literature examples concerning the formation of titania nanoparticles produce the crystallinity via subsequent calcining (e.g. Fernández-Garcı et al., 2007; Fresno et al., 2009) or a combined microemulsion-solvothermal process (e.g. Kong et al., 2011). Many methods also involve continual stirring. This is not necessary for microemulsions since they are thermodynamically stable, and stirring may disrupt any potential thermodynamic control if larger transient droplets are formed from multiple colliding droplets. Our microemulsion methodology enables direct crystallization of the nanocrystals of rutile, the stable form of titania, at room temperature provided the solute concentrations are kept sufficiently low and the crystallization is confined (predominantly) to the dispersed phase. To illustrate this, a microemulsion comprising 1.74 g of cyclohexane, 1-hexanol and Triton X-100 in the volume ratio of 7 : 1.2 : 1.8, and 180 μl of 2M HCl as the dispersed phase, was prepared. To this was added a solution of 180 μl of titanium isopropoxide (TIPO) in 1.74 g of the cyclohexane, 1-hexanol and Triton X-100 surfactant solution. The TIPO molecules reacted with the water predominantly at the droplet interface so that the resulting titanium dioxide resided mainly in the droplets. The use of 2M HCl slowed down the production of titanium dioxide, preventing gellation, and allowing the crystallization to proceed under thermodynamic control to give the stable rutile phase. TEM after 12 hours confirmed that the nanoparticles of size ~4 nm were crystalline rutile (see Figure 10a). After 3 days the nanocrystals were ~100 nm (see Figure 10b).

Similar microemulsion compositions with surfactant:aqueous mass ratios of 2.5:1 or less and ≤9% by volume of TIPO, produced rutile nanoparticles of good crystallinity. Indeed calcining these particles at 450 ˚C for 18 hours led to only a small increase in crystallinity (see Figure 10c). The microemulsions gradually took on a blue tinge over several days due

to scattering from the growing rutile particles. The growth of the nanoparticles could be increased by the subsequent addition of water to swell the droplets so that an emulsion formed. Notably, even if the water addition occurred only a few minutes after mixing the TIPO solution with the aqueous HCl microemulsion, good crystallinity rutile particles were still formed. In contrast, when the reaction was carried out in the bulk phase, poor crystallinity/amorphous titania was obtained, demonstrating that the microemulsion stage was crucial for the formation of seed rutile nanocrystals. This general strategy of slowing the reaction rate via limited reactants and/or an appropriate pH range can be used to help introduce, or increase, crystallinity of inorganic nanoparticles obtained from microemulsions.

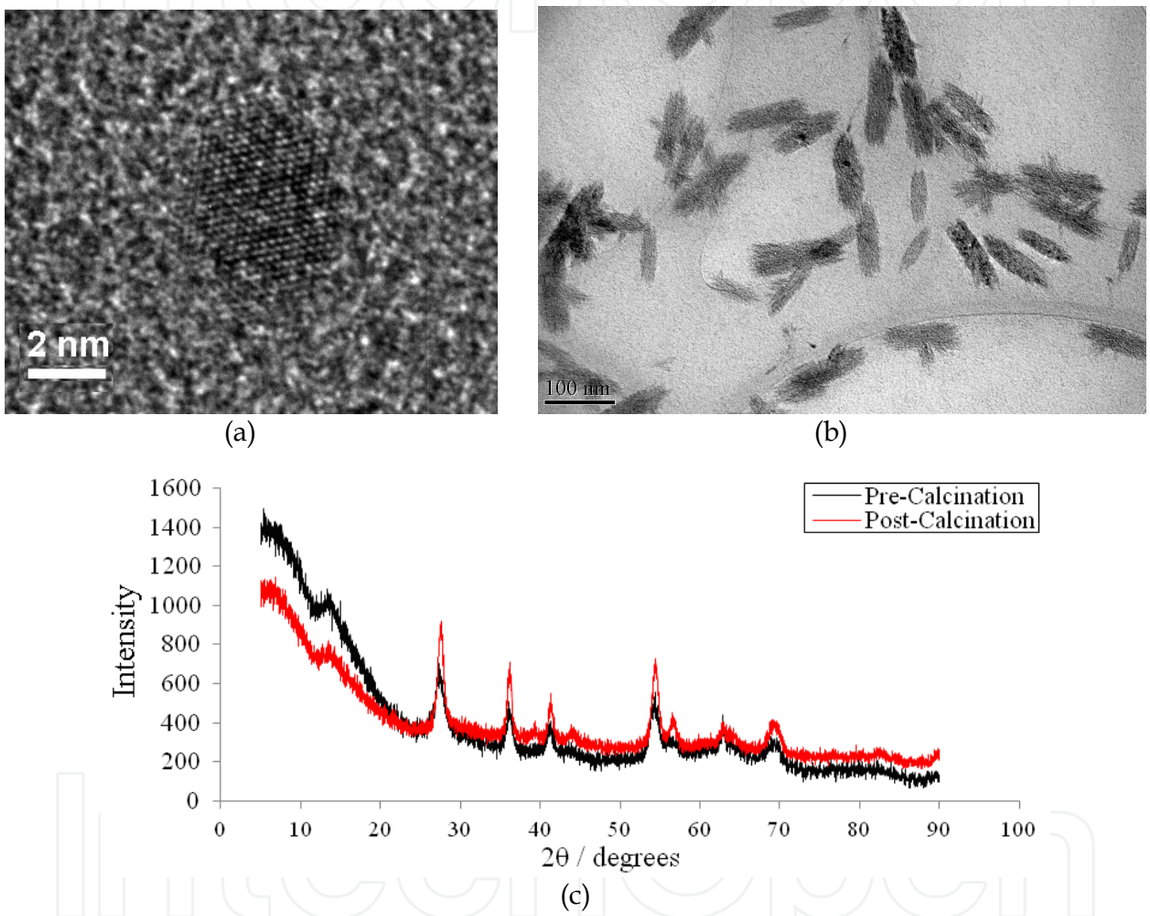


Fig. 10. Crystallization of rutile from microemulsions at room temperature and pressure. (a) High resolution electron microscopy image showing a 4 nm nanocrystal grown after 12 hours. (b) Electron microscopy image of the rutile nanocrystals taken after 3 days. (c) Powder X-ray diffraction trace of the rutile nanocrystals before and after calcination.

4.5 Advantages and drawbacks of crystallization in microemulsions

The use of microemulsions to exert thermodynamic control of crystallization is clearly an advantage whenever stable crystal forms are needed, such as in drug formulations and in obtaining nanocrystals with specific size-dependant properties. However, the much slower growth of crystals in microemulsions, compared to that in bulk solution, may limit

industrial applications. A strategy whereby the microemulsion is controllably destabilized once the (near) stable nuclei have formed may circumvent this problem. For instance, the addition of more dispersed phase to swell the droplets into an emulsion may prove advantageous, provided the additional solution results in growth only on the existing (near) stable nuclei and nanocrystals, rather than the nucleation of new crystals, since the latter would be produced under kinetic, rather than thermodynamic, control. An effective approach to ensure this would be to induce the supersaturation of the additional dispersed phase slowly only after the emulsion has formed e.g. by cooling or adding a separate microemulsion containing an antisolvent.

5. Conclusion

Microemulsions present a unique opportunity for both the reliable estimate of critical nucleus sizes and the thermodynamic control of crystallization. The 3D droplet nanoconfinement results in crystallization being limited by the ability to form (near) stable nuclei, rather than critical nuclei, under conditions where crystallization is only just possible. This is a direct consequence of the limited amount of material within a droplet. In solution crystallization there is a substantial supersaturation decrease as a nucleus grows in a nanodroplet. The supersaturation decrease means that very high initial supersaturations are required in a droplet to achieve a (near) stable nucleus, thus enabling nucleation barriers to be readily surmountable. Hence solution crystallization from microemulsions is the only methodology known to-date that can generically crystallize stable polymorphs directly, even when they have insurmountable nucleation barriers in bulk solution. The transient dimer formation in microemulsions provides a mechanism for nuclei growth; we find it is possible to grow crystals ranging from nm to mm in size. Crystallization in microemulsions has already been successfully applied to 'leapfrog' Ostwald's rule of stages and directly crystallize the stable polymorphs of three 'problem' organic systems: glycine, mefenamic acid and ROY. The methodology should be of significant use in the pharmaceutical industry, as it provides the first generic method for finding the most stable polymorph for any given drug, thereby preventing another Ritonavir-type crisis. Microemulsions have also been used to synthesis nanocrystals of rutile without requiring a subsequent calcination step. Other inorganic systems that typically produce amorphous nanoparticulates are also likely to benefit from this approach. Its application to protein crystallization may prove problematic, given the larger size of protein molecules, though droplet clustering to fully encase the protein may occur in these systems alleviating this limitation. Future work will investigate this possibility. A disadvantage of the methodology is that once the (near) stable nuclei are generated, their growth is significantly impeded. Initially this is due to their nanoconfinement, and subsequently, when the nanocrystals grow bigger than these droplets, results from the limited concentration of their molecules in the continuous phase. Controlled microemulsion destabilization strategies, such as adding more of the dispersed phase to form an emulsion, may prove a viable route to circumvent this problem. Finally, given that the ultimate crystal size can vary from nm to mm, depending upon the population of (near) stable nuclei and their subsequent growth rates, there is a significant need for greater understanding of how the growth rates can be tuned. Then the use of microemulsions in crystallization would be truly unrivalled in producing both high crystallinity forms and the desired crystal size.

6. Acknowledgement

We thank EPSRC for funding.

7. References

Allen, K.; Davey, R. J.; Ferrari, E.; Towler, C. & Tiddy, G. (2002). The Crystallization of Glycine Polymorphs from Emulsions, Microemulsions and Lamellar Phases. *Crystal Growth & Design.,* Vol. 2, No. 6 (November, 2002), pp523-527.

Bartell, L. S. (1998). Structure and Transformation: Large Molecular Clusters as Models of Condensed Matter. *Annu. Rev. Phys. Chem.*, Vol. 49, (October 1998), pp43-72.

Becker, R. & Döring, W. (1935). Kinetic Treatment of Germ Formation in Supersaturated Vapour *Ann. Phys.*, Vol. 24, No. 8, (December 1935), pp719-752.

Bowles, R. K.; Reguera D.; Djikaev Y. & Reiss H. (2001). A Theorem for Inhomogeneous Systems: The Generalization of the Nucleation Theorem. *Journal o Chemical Physics*, Vol. 115, (July 2001) pp1853-1866.

Bowles, R. K.; Reguera D.; Djikaev Y. & Reiss H. (2002). Erratum: A Theorem for Inhomogeneous Systems: The Generalization of the Nucleation Theorem. *Journal of Chemical Phyics*, Vol. 116, (February 2002) pp2330.

Chemburkar, S. R.; Bauer, J.; Deming, K.; Spiwek, H.; Patel, K.; Morris, J.; Henry, R.; Spanton, S.; Dziki, W.; Porter, W.; Quick, J.; Bauer, P; Donaubauer, J.; B.; Narayanan, B. A.; Soldani, M.; Riley, D. & McFarland, K. (2000). Dealing with the Impact of Ritonavir Polymorphs on the Late Stages of Bulk Drug Process Development. *Organic Process Research & Development*, Vol. 4, No. 5 (June 2000), pp413-417.

Chen C.; Cook, O.; Nicholson C. E. & Cooper S. J. (2011). Leapfrogging Ostwald's rule of stages: Crystallization of stable γ-glycine directly from microemulsions. *Crystal Growth & Design,* Vol. 11, No. 6 (April 2011), pp2228-2237.

Chew, J. W.; Black, S. N.; Chow, P. S.; Tan, R. B. H. & Carpenter, K. J. (2007). Stable Polymorphs: Difficult to Make and Difficult to Predict. *Crystal Engineering Communications* Vol. 9, No. 2 (January 2007), pp128-130.

Clausse, D.; Babin, L.; Broto, F.; Aguerd, M. & Clausse, M. (1983). Kinetics of Ice Nucleation in Aqueous Emulsions. *Journal of Physical Chemistry* Vol. 87, No. 21 (October 1983), pp4030-4034.

Cooper, S. J.; Nicholson, C. E. & Lui, J. (2008). A simple classical model for predicting onset crystallization temperatures on curved substrates, and its implications for phase transitions in confined volumes. *Journal of Chemical Physics* Vol. 129, No. 12 (September 2008), 124715.

Couchman, P. R. & Jesser, W. A. (1977). Thermodynamic Theory of Size Dependance of Melting Temperature in Metals. *Nature*, Vol. 269, No. 5628, (October 1977), pp481-483.

Denoyel, R. & Pellenq R. J. M. (2002). Simple Phenomenological Models for Phase Transitions in a Confined Geometry. 1: Melting and Solidification in a Cylindrical Pore. *Langmuir,* Vol. 18, No. 7, (April 2002), pp2710-2716.

Erdemir, D.; Lee, A. Y. & Myerson, A. S. (2009). Nucleation of Crystals from Solution: Classical and Two-Step Models. *Accounts of Chemical Research*, Vol. 42, No. 5, (May 2009), pp621-629.

Eriksson, J. C. & Ljunggren, S. (1995). Comments on the Alleged Formation of Bridging Cavities/Bubbles Between Planar Hydrophobic Surfaces. *Langmuir,* Vol. 11, No. 6, (Month 1995), pp1145-1153.

Fletcher N. H. (1958). Size Effect in Heterogeneous Nucleation. *Journal of Chemical Physics*, Vol. 29, No. 3, (May 1958), pp572-576.

Fernández-Garcıa, M.; Belver, C.; Hanson, J. C.; Wang, X. & Rodriguez, J. A. (2007). Anatase-TiO2 Nanomaterials: Analysis of Key Parameters Controlling Crystallization. *Journal of the American Chemical Society*, Vol. 129, No. 44, (January 2007), pp13604-13612.

Fresno, F.; Tudela, D.; Coronado, J. M. & Soria J. (2009). Synthesis of Ti1_xSnxO2 nanosized photocatalysts in reverse microemulsions. *Catalysis Today*, Vol. 143, No. 3-4 (May 2009), pp230–236.

Füredi-Milhofer, H.; Garti, N. & Kamyshny, A. (1999). Crystallization from microemulsions - a novel method for the preparation of new crystal forms of aspartame. *Journal of Crystal Growth*, Vol. 198, (March 1999), pp1365-1370.

Ganguli, A. K.; Ganguly A. & Vaidya, S. (2010). Microemulsion-based Synthesis of Nanocrystalline Materials. *Chemical Society Reviews,* Vol. 39, No. 2, (January 2010), pp474–485.

Gibbs, J. W. (1876). On the equilibrium of heterogeneous substances. *Trans. Connect. Acad. Sci.*, Vol. 3, pp108–248.

Gibbs, J. W. (1878). On the equilibrium of heterogeneous substances. *Trans. Connect. Acad. Sci.*, Vol. 16, pp343–524.

Kashchiev, D. (1982). On the Relation Between Nucleation Work, Nucleus Size and Nucleation Rate. *Journal of Chemical Physics*, Vol. 76, No. 10, (May 1982), pp5098-5102.

Jamieson, M. J.; Nicholson, C. E. & Cooper, S. J. (2005). First Study on the Effects of Interfacial Curvature and Additive Interfactial Density on Heterogeneous Nucleation. Ice Crystallization in Oil-in-Water Emulsions and Nanoemulsions with Added 1-heptacosanol. *Crystal Growth & Design*, Vol. 5, No. 2, (March 2005), pp451-459.

Kong, W.; Liu, B.; Ye, B.; Yu, Z.; Wang, H.; Qian, G. & Wang, Z. (2011) An Experimental Study on the Shape Changes of TiO2 Nanocrystals Synthesized by Microemulsion-Solvothermal Method, *Journal of Nanomaterials* Volume 2011, Article ID 467083, 6 pages.

Liu, J.; Nicholson, C. E. & Cooper, S. J. (2007). Direct measurement of critical nucleus size in confined volumes. *Langmuir,* Vol. 23, No. 13, (June 2007), pp7286-7292.

Nicholson, C. E.; Chen, C.; Mendis, B. & Cooper, S. J. (2011) 'Stable Polymorphs Crystallized Directly under Thermodynamic Control in Three-Dimensional Nanoconfinement: A Generic Methodology' *Crystal Growth & Design*, Vol 11, No. 2 (February 2011), pp. 363-366.

Nicholson, C. E. & Cooper, S. J. (2011). Crystallization of Mefenamic Acid from DMF Microemulsions: Obtaining Thermodynamic Control through 3D Nanoconfinement. *Crystals* Vol. 1, No. 3, (September 2011), pp. 195-205.

Nicholson, C. E.; Cooper, S. J.; Marcellin, C. & Jamieson, M. J. (2005). The Use of Phase-Inverting Emulsions to Show the Phenomenon of Interfacial Crystallization on both Heating and Cooling. *Journal of the American Chemical Society,* Vol. 127, No. 34, (August 2005), pp11894-11895.

Ostwald, W. Z. (1897). Studies of the Formation and Transformation of solid Substances. *Zeitschrift für Physikalische Chemie*, Vol. 22, (1897), pp289-330.

Oxtoby, D. W. & Kashchiev, D. (1994). A General Relation Between the Nucleation Work and the Size of the Nucleus in Multicomponent Nucleation. *Journal of Chemical Physics*, Vol. 100, No. 10, (May 1994), pp7665-7671.

Petit, C.; Lixon, P. & Pileni, M. P. (1990). Synthesis of Cadmium Sulfide in situ in Reverse Micelles. 2: Influence of the Interface on the Growth of the Particles. *Journal of Physical Chemisty*, Vol. 94, No. 4, (February 1990), pp1598–1603.

Petrov, O. & Furó, I. (2006). Curvature-dependant Metastability of the Solid Phase and the Freezing-Melting Hysteresis in Pores. *Phyical Reiew E*, Vol. 73, No. 1, (January 2006), 001608-1 – 001606-7.

Popovitz-Biro, R.; Wang, J. L.; Majewski, J.; Shavit, E.; Leiserowitz, L.; Lahav, M. (1994). Induced Freezing of Supercooled Water into Ice by Self-Assembled Crystalline Monolayers of Amphiphilic Alcohols at the Air-Water Interface. *Journal of the American Chemical Society,* Vol. 116, No. 4, (February 1994), pp1179-1191.

Pruppacher, H. R. (1995). A New Look at Homogeneous Ice Nucleation in Supercooled Water Drops. *Journal of Atmospheric Science*, Vol. 52, No. 11, (June 1995), pp1924-1933.

Reguera, D.; Bowles, R. K.; Djikaev Y. & Reiss, H. (2003). Phase Transitions In Systems Small Enough to be Clusters. *Journal of Chemical Physics*, Vol. 118, No. 1, (January 2003), pp340-353.

Speedy, R. J. (1987). Thermodynamic Properties of Supercooled Water at 1 atm. *Journal of Phyical Chem*istry, Vol. 91, No. 12, (June 1987), pp3354-3358.

Vanfleet, R. R. & Mochel, J. M. (1995). Thermodynamics of Melting and Freezing in Small Particles. *Surf. Sci.*, Vol. 341, No. 1-2, (November 1995), pp40-50.

Vekilov, P. G. (2010). Nucleation. *Crystal Growth & Design,* Vol. 10, No. 12, (December 2010), pp5007–5019.

Volmer, M, & Weber, A. (1926). Germ Formation in Oversaturated Figures. *Zeitschrift fürPhysikalische Chemie*, Vol. 119, No. 3-4, (March 1926), pp277-301.

Wood, G. R. & Walton, A. G. (1970). Homogeneous Nucleation Kinetics of Ice from Water. *Journal of Applied Physics*, Vol. 41, No. 7 (June 1970), pp3027-3036.

Xu, D. & Johnson, W. L. (2005). Geometric Model for the Critical-Value Problem of Nucleation Phenomena Containing the Size Effect of Nucleating Agent. *Physical Review B*, Vol. 72, No. 5, (August 2005), pp052101.

Yano, J.; Füredi-Milhofer, H.; Wachtel, E. & Garti, N. (2000). Crystallization of Organic Compounds in Reversed Micelles. 1: Solubilization of Amino Acids in Water-

Isooctane-AOT Microemulsions. *Langmuir*, Vol. 16, No. 26, (December 2000), pp10005-10014.

Zarur, A. J. & Ying, J.Y. (2000). Reverse Microemulsion Synthesis of Nanostructured Complex Oxides for Catalytic Combustion. *Nature*, Vol. 403, No. 6765, (January 2000), pp65–67.

IntechOpen

IntechOpen

© 2012 The Author(s). Licensee IntechOpen. This is an open access article distributed under the terms of the Creative Commons Attribution 3.0 License, which permits unrestricted use, distribution, and reproduction in any medium, provided the original work is properly cited.

IntechOpen

IntechOpen